Article

Electrostatic Acoustic Sensor with an Impedance-Matched Diaphragm Characterized for Body Sound Monitoring

Valerie Rennoll, Ian McLane, Adebayo Eisape, Drew Grant, Helena Hahn, Mounya Elhilali, and James E. West*

Cite This: ACS Appl. Bio Mater. 2023, 6, 3241−3256 | Read Online

ACCESS | Metrics & More | Article Recommendations | SI Supporting Information

ABSTRACT: Acoustic sensors are able to capture more incident energy if their acoustic impedance closely matches the acoustic impedance of the medium being probed, such as skin or wood. Controlling the acoustic impedance of polymers can be achieved by selecting materials with appropriate densities and stiffnesses as well as adding ceramic nanoparticles. This study follows a statistical methodology to examine the impact of polymer type and nanoparticle addition on the fabrication of acoustic sensors with desired acoustic impedances in the range of 1−2.2 MRayls. The proposed method using a design of experiments approach measures sensors with diaphragms of varying impedances when excited with acoustic vibrations traveling through wood, gelatin, and plastic. The sensor diaphragm is subsequently optimized for body sound monitoring, and the sensor's improved body sound coherence and airborne noise rejection are evaluated on an acoustic phantom in simulated noise environments and compared to electronic stethoscopes with onboard noise cancellation. The impedance-matched sensor demonstrates high sensitivity to body sounds, low sensitivity to airborne sound, a frequency response comparable to two state-of-the-art electronic stethoscopes, and the ability to capture lung and heart sounds from a real subject. Due to its small size, use of flexible materials, and rejection of airborne noise, the sensor provides an improved solution for wearable body sound monitoring, as well as sensing from other mediums with acoustic impedances in the range of 1−2.2 MRayls, such as water and wood.

KEYWORDS: acoustic sensor, body sound monitoring, acoustic impedance matching, sensor design, biomedical acoustics

INTRODUCTION

Sensors for sound capture have wide-ranging characteristics based on the application, desired transduction method, frequency range of interest, required sensitivity, and medium being monitored. The medium being monitored is critical because it has a specific acoustic impedance (Z), a material property related to the density, and speed of sound, that opposes longitudinal wave motion.[1] When sound intersects at the interface between the medium being monitored and sensor, the pressure and velocity of the incident wave must equal the sum of the pressure and velocity of the transmitted and reflected waves. When there is an acoustic impedance mismatch, this leads to partial energy transmission between the medium and sensor.[2] To capture as much acoustic energy as possible, sensors with an acoustic impedance similar to the medium being probed are preferred. While acoustic impedance matching has been studied extensively in both underwater and ultrasound[3] applications, there is less research outside of these applications, and in particular, for monitoring body sounds.

Sensors with acoustic impedance matching for monitoring lung and heart sounds could be particularly impactful because these mechano-acoustic physiological signals at the surface of

the skin are relatively weak, especially with increasing frequency.[4] When these sounds travel from the body ($Z \approx 1.53−1.68$ MRayls[5]) to air ($Z = 0.0004$ MRayls[6]), 99.9% of the incident signal energy is reflected at the boundary due to the acoustic impedance mismatch. In acoustic stethoscopes, which are used to pick up these weak signals, the diaphragm acts as a matching and amplifying layer, transmitting more energy to air such that it can travel through tubing to the ears of the user.[7] Although the acoustic stethoscope diaphragm amplifies weak physiological signals, it is also susceptible to airborne noise, which can severely corrupt the body sound of interest and limit clinical usability in noisy environments.[8]

Electronic stethoscopes similarly use coupling to the chest with a diaphragm and then sensitive transducers to capture the generated vibrations or airborne sound in a chamber, followed

by amplification to increase the functional signal for the user. Currently, there are a variety of sensor types used in stethoscopes, namely, electret condenser microphones, micro-electromechanical system (MEMS) microphones, and piezo-electric transducers.[9,10] Although these sensors have the required sensitivity to capture body sounds, they still face limitations such as susceptibility to airborne noise, high internal noise levels, and costly fabrication processes.[10] Several studies have proposed noise suppression solutions to overcome the airborne noise susceptibility of stethoscopes,[11,12] but such approaches could alter the original body sound content and require substantial processing power. The airborne noise susceptibility and rigid form factor of current stethoscopes are two limiting factors that inhibit wearable and continuous body sound capture for monitoring respiratory and cardiac diseases.

An alternative method to monitor body sound vibrations is to use a contact sensor, such as an accelerometer, on the skin. An accelerometer only measures the surface to which it is attached and is theoretically insensitive to the surrounding air pressure oscillations. These small and lightweight transducers are typically in rigid electronic packages and physically strapped on the body to couple with the skin.[13,14] However, recent advances in soft electronics have led to skin-compliant devices that incorporate accelerometers to capture cardiac mechanics, such as seismocardiograms or ballistocardio-grams,[15] and respiration.[16] Though these approaches have become increasingly common, there are several challenges for capturing lung sounds specifically. Traditional accelerometers and inertial measurement units typically have a low frequency range (<1 kHz); as frequency increases, the sensitivity decreases and measurement uncertainty increases.[17] As such, accelerometers are most effective at low frequencies (0−100 Hz), which is adequate for capturing S1 and S2 cardiac sounds and sub-Hz respiration signals. However, the limited high frequency pickup restricts their use for capturing respiratory sounds which contain clinically relevant information in higher frequencies. Many accelerometers also face challenges with the minimum detectable acceleration due to the resolution and internal noise floor. More subtle physiological signals—S3 and S4 heart sounds and most lung sounds—have amplitudes that can be an order of magnitude lower than the milli-gravity (mg) sensitivity of most accelerometers and would suffer from interference or masking.[18,19] Overall, accelerometers are limited for body sound pickup because they only capture skin vibration, which is a crude and low-pass version of the actual acoustic signal emanating from the lungs or heart.

Outside of these existing solutions, there have been several proposed new device designs that would enable comfortable and continuous health monitoring via acoustic signals.[10,20] One general approach is to combine a typical off-the-shelf microphone with an acoustic impedance matching layer,[21−23] which improves the device sensitivity and noise rejection. Several studies have also used off-the-shelf accelerometers with encapsulation in an elastomer that incorporates soft and stretchable electronics,[13,24] while another developed a new ultrasensitive and wideband accelerometer that cannot be fabricated with conventional methods.[25] Similarly, a third general approach is to incorporate polymeric or ceramic piezoelectric materials in various form factors such as a thin, serpentine layout,[26] curved film with supporting elastomeric layer,[27] rigid printed circuit board (PCB) with silicone packaging and air gap,[28] or a ceramic beam.[29] Triboelectric nanogenerators are also becoming increasingly common,[30] but

they demonstrate limited stability and durability,[30] and are typically focused on capturing respiration rate rather than full lung sounds[31] or heart or pulse rate.[32] Other less common approaches have included a bionic sensor structure inspired by the human ear[33] and a sensor that uses an electrochemical reaction for transduction.[34] The majority of these approaches either disregard acoustic impedance matching or incorporate it by using a polymer as a coupling or encapsulation layer that interfaces with a separate transduction device.

Compared to these approaches, the goal of this study was to place acoustic impedance matching at the forefront of the sensor design by introducing a diaphragm with a precisely controlled acoustic impedance. In addition to this primary goal, secondary aims also included incorporating the desired characteristics (high sensitivity to body sounds, low sensitivity to airborne sounds, broad bandwidth, flexible materials, small size) and minimizing the drawbacks (complicated fabrication methods, encapsulated liquids, large and rigid components) of existing approaches. The basic proposed acoustic impedance-matched sensor (AIMS) design is based around the electro-static interactions that occur between a charged electret polymer and an impedance-matched polymer with metal-coated microstructures held together in a capacitive structure. By matching the mechanical and acoustical properties of the sensor to the body, the energy transmitted to the sensor from the body will be maximized, while corruption from airborne noise will be minimized. While similar to the structure of triboelectric sensors presented previously,[31] the charged electret film in the AIMS is expected to provide the increased sensitivity required for capturing subtle physiological signals. Overall, the main aims of this study are to (1) develop a generalized statistical model that connects the relationship between multiple fabrication and characterization conditions to the acoustic impedance and attenuation of several polymers, (2) use this model to construct the AIMS diaphragm and quantify the impact impedance matching has on the sensor response, and (3) demonstrate the improved signal fidelity and noise rejection of the AIMS under conditions that mimic body sound monitoring.

To incorporate the acoustic impedance-matched diaphragm, several previous studies have shown that the acoustic impedance can be tuned based on the polymer type and added ceramic particles.[35−38] However, previous work typically focused on varying a single parameter at a time. This approach is useful when determining how to match only a single impedance value but does not account for interactions that occur between multiple variables. To understand how the diaphragm could be tuned to match the acoustic impedance of skin, as well as other materials like water and wood, the study begins by developing a model using a design of experiments approach to specify the conditions necessary for fabricating a polymer with a specific acoustic impedance and minimum attenuation. To demonstrate that the acoustic impedance of the diaphragm does indeed impact acoustic transmission through materials with varying acoustic impedances and therefore the AIMS output, an acoustic phantom with different material layers excites (1) polymers with a range of acoustic impedances and (2) AIMS with varying impedances. The average responses measured by a laser vibrometer or the AIMS from various materials are shown to be proportional to the acoustic velocity or pressure transmission coefficients. Building on the generalized sensor design, an AIMS with a diaphragm specifically matching skin is fabricated and characterized for its
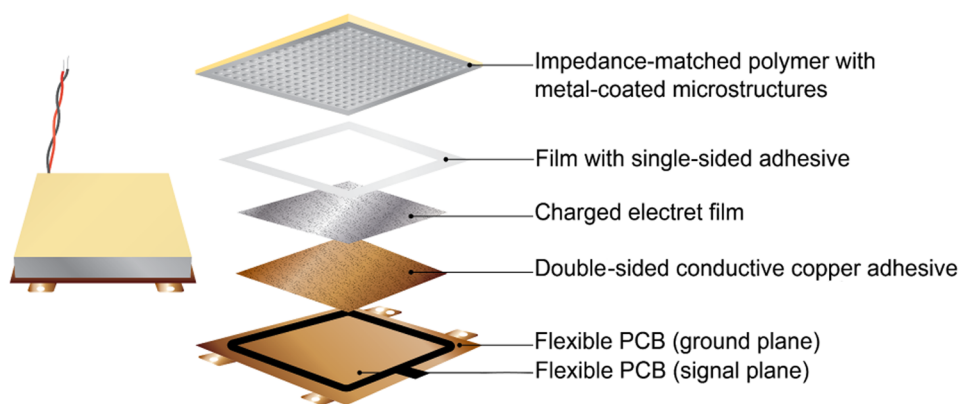
Figure 1. Schematic showing the capacitive structure of the AIMS with three main components—an impedance-matched polymer, metal-coated microstructures, and a charged electret film.

electrical response with various excitations, stability over time, and with temperature, frequency response, signal fidelity, and noise rejection. To our knowledge, this is the first study that generates a validated statistical model to predict the acoustic impedance of polymers and introduces acoustic impedance matching into a sensor diaphragm without matching layers. While this study will concentrate on monitoring body sounds, the AIMS has the potential to be tuned for sensing in other mediums as well.

MATERIALS AND METHODS

Transducer Design and Fabrication. The AIMS, schematically shown in Figure 1, was designed with a capacitive structure and three main components—an impedance-matched polymer, metal-coated microstructures, and a charged electret film. The electret film traps charges quasi-permanently and generates a permanent electric field.[39] The microstructures create an air gap between the polymer diaphragm and electret layer, such that the metal coating on the microstructures and the metal backing of the electret film form a capacitor. The capacitance is a function of the electret film surface area and the change in the height of the microstructures in the AIMS. When a mechanical vibration is incident on the polymer, the microstructures are deformed, which changes the distance between the grounded electrode on the surface of the microstructures and the back of the charged electret film. The varying microstructure height changes the capacitance, generating an electrical response.

To construct the AIMS, a flexible printed circuit board (PCB) (23×23 mm^2) was manufactured (PCBWay, Shenzhen, China) with two metalized areas on the functional surface to serve as ground and signal planes, as well as a ground plane on the back surface for isolation from electrical noise. The metalized side of a fluorinated ethylene propylene (FEP) electret film ($17 \times 17 \times 0.01$ mm^3) was adhered to the center of the PCB (on the signal plane) using double-sided, conductive copper adhesive (3M 1182). The film and PCB were hot-pressed together using a mini manual heat press at 93 °C for 120 s and allowed to cool. A 0.04 mm thick polypropylene film frame (18×18 mm^2 square with 14 mm × 14 mm cutout) with adhesive backing was placed surrounding the FEP to prevent electrical shorting between the ground and signal planes in the final AIMS construction. The PCB with attached FEP was grounded within a laboratory corona charging setup (shown in Figure S1) and charged with a grid voltage of 1500 V and tip voltage of 20 kV for approximately 10 min at 80 °C. The sample was allowed to cool to room temperature before removing the applied voltage. After charging, the presence of charges was confirmed using an electrostatic voltmeter (Monroe Electronics model 279).

To form the acoustic impedance-matched diaphragm, a polymer with the desired acoustic properties, as discussed in the section "Demonstrating the Effect of Acoustic Impedance Matching", was poured into a mold with conical indents that have a 250 μm diameter and 270 μm height and are placed 250 μm apart. The polymer was degassed for approximately 20 min to minimize air bubbles and allowed to cure to a final size of approximately $22 \times 22 \times 2$ mm^3. For body sound monitoring specifically, a polyurethane diaphragm was used as its measured acoustic impedance (≈ 1.54 MRayls) is well within the range of the body ($Z \approx 1.53-1.68$ MRayls). The side of the polymer with the conical microstructures was airbrushed with a conductive, silicone-based ink (Creative Materials 125-19FS) and allowed to dry. Conductivity across the polymer surface was confirmed using a multimeter.

The metal-coated polymer and PCB with charged FEP were placed together, held in place using a 100 g weight, and adhered at the edges using a permanent adhesive (Loctite Super Glue). The metal-coated polymer was attached to the outer ground plane of the PCB, such that the AIMS was grounded from electrical noise. For acoustic characterization, an amplifier with a junction-gate field-effect transistor (JFET, Toshiba 2SK879) and 1 kΩ resistor were soldered directly to the PCB. Otherwise, the voltage output of the AIMS was measured directly from the signal and ground planes. The final sensor, which weighs approximately 1.55 g, is shown in Figure S2.

Design of Experiments. An I-optimal design was used to develop a model that predicts the conditions necessary to fabricate the polymer diaphragm with a specific acoustic impedance and minimal attenuation. Seven factors were studied, including the polymer type, particle density, concentration, and size, sample thickness, and characterization frequency and temperature, as shown in Table 1. The responses included the measured acoustic impedance and attenuation. JMP software[40] was used to generate the I-optimal design based on the given factors and constraints. A total of 98 samples were prepared to have reasonable statistical power to detect all main effects, second-order interactions, and quadratic terms for

Table 1. Factors and Factor Levels Used in the Design of Experiments to Understand How to Fabricate a Polymer Diaphragm with a Specific Acoustic Impedance and Minimal Attenuation

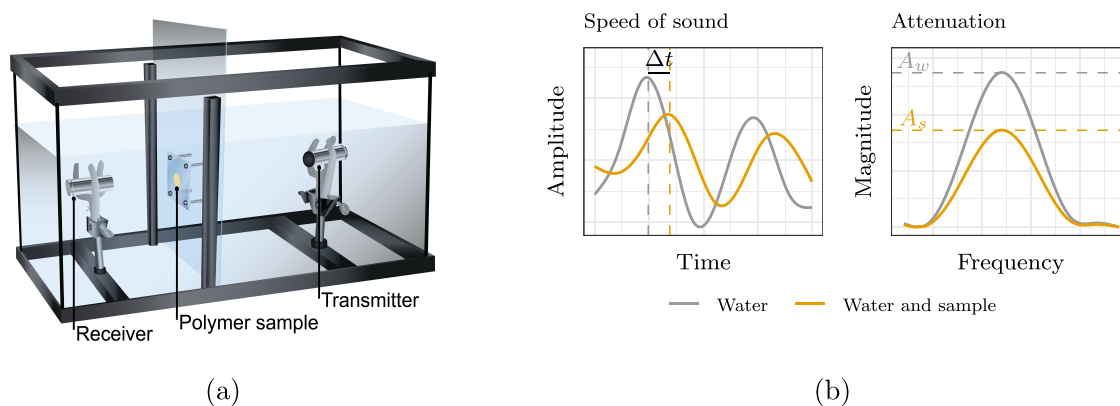| factor	levels
polymer type	PDMS (10:1), PDMS (20:1), Ecoflex, polyurethane
particle density (10^3 kg/m^3)	2.2 (SiO$_2$), 3.89 (TiO$_2$), 6.02 (BaTiO$_3$)
particle concentration (wt %)	0, 25, 50
average particle size (nm)	150, 450, 1000
sample Thickness (mm)	2, 6, 10
characterization frequency (MHz)	0.8, 1.2, 1.6
characterization temperature (°C)	15, 20, 25, 30, 35

Figure 2. Through-transmission technique was used for acoustic characterization; (a) schematic of the setup with an ultrasonic transmitter and receiver placed on either side of the sample in a tank of water and (b) time shift and amplitude shift that can be measured for speed of sound and attenuation calculations.

modeling the desired responses. More information on the choice of factors and their levels, as well as the specific treatment conditions, is included in the Supporting Information.

In general, each polymer sample, poly(dimethylsiloxane) (PDMS), Ecoflex, or polyurethane, was fabricated by hand mixing a certain concentration by weight of added particles with the correct ratio of polymer components. Ecoflex and polyurethane were prepared with equal parts A and B by weight, while PDMS was prepared in ratios of 10:1 and 20:1. In each case, the particles were added and mixed with part A prior to the addition of part B. The resulting mixture was degassed to remove air bubbles and poured into a circular 44 mm diameter nylon mold with a thickness of 2, 6, or 10 mm. Samples were allowed to cure at room temperature or in an oven (Thermo Scientific Lindberg Blue M), based on the polymer type. Detailed information on each polymer and its fabrication is provided in the Supporting Information.

Polymer Acoustic Impedance and Attenuation Characterization. After curing, the density (ρ_s), speed of sound (SoS$_s$), acoustic impedance (Z_s), and attenuation (α_s) of each polymer sample from the design of experiments was measured. Density was calculated as the sample mass-to-volume ratio. Mass was measured using a digital scale (A&D GF-200) and averaged over eight separate measurements. Volume was measured using a suspension method based on Archimedes' principle where a sample is immersed in water, and the change in mass is recorded.[41] The volume (V_s) was calculated as

$$V_s = \frac{\Delta w}{\rho_w} \qquad (1)$$

where Δw is the change in mass recorded by the scale when the sample was fully suspended in water and ρ_w is the density of water. The water temperature was approximated as 20 °C, such that the density of water was calculated as 997.989 kg/m^3.[42] Each sample volume was averaged over five separate measurements.

The speed of sound and attenuation of the samples were measured using the relative through-transmission technique, which determines the unknown acoustic properties of the sample under test in comparison to water.[43] This method involves positioning the sample of interest between an ultrasonic transmitter and receiver in a tank of water, as shown schematically in Figure 2a and with an image in Figure S3. The signals transmitted between the transducers are compared when traveling through water alone versus both the sample and water. While there are several sources of uncertainty (namely, thickness and temperature measurements and instrumentation resolution)[44,45] present in the through-transmission technique and other approaches[44,46−48] are studied for measuring the speed of sound and attenuation, the method provides a simplistic way to compare a large number of samples and has been used previously in numerous studies[36−38,49] allowing for measurement comparisons to other

researchers. Madsen et al.[50] coordinated researchers from seven different universities to measure the same material using the through-transmission technique and found that the speed of sound and attenuation had spreads within 0.3 and 20%, respectively, indicating that attenuation measurements are more variable due to the uncertainty sources present. Prior to measuring samples for the design of experiments, the density and through-transmission measurement techniques were validated using various materials, including PDMS, castor oil, and pig skin and heart tissues, as shown in the Supporting Information (Figures S4−S6 and Tables S2−S4).

Ultrasonic probes (Goworld 2.5P) with a center frequency of 2.5 MHz and 14 mm element size were used to transmit and receive signals. The transducers were aligned and fixed to a welded base in a 10 gallon glass aquarium. An acrylic sheet with a 2 cm diameter cutout for the polymer sample was placed 25 cm from the transmitting probe and 7.5 cm from the receiving probe such that the polymer being measured was in the far field of the transmitter for the frequencies emitted. The sample being measured was held tightly against the acrylic centerpiece using a spring mechanism that evenly applied pressure to the outer edges of the sample. Prior to taking measurements, each sample was submerged in water and allowed approximately 15 min to equilibrate to the temperature of the water as monitored by a temperature controller (Inkbird ITC-308). The transducer was driven by a function generator (Tektronix AFG 3022B) to emit a specific signal. A graphical user interface (shown in Figure S7) remotely controlled both the function generator and oscilloscope to emit and record the transducer signals. To reduce random effects related to water bubbles and impurities, measurements for the speed of sound and attenuation were repeated in three different water baths but with all other experimental conditions the same. In each water bath, a sample was measured a total of four times, twice from both the front and back, for a total of 12 measurements per sample that were averaged.

To determine the speed of sound, a tone burst with a 10 V peak-to-peak amplitude and frequency of 0.8, 1.2, or 1.6 MHz was generated by the function generator and emitted by the transmitter. The time shift between the signal at the receiver when the tone burst traveled through water alone versus the sample and water was measured, as shown in the left panel of Figure 2b. Using this measured time shift, the speed of sound through the sample was calculated using the following equation

$$SoS_s = \frac{h}{\Delta t + \frac{h}{SoS_w}} \qquad (2)$$

where h is the average sample thickness, Δt is the time shift, and SoS$_w$ is the speed of sound in water.[38] The sample thickness was measured using calipers at nine randomly chosen positions and averaged. The time shift between a single measurement of the signal transmitted through water alone and four measurements of the signal through

water and the sample was determined via cross correlation. The speed of sound in water was calculated based on the measured water temperature, assuming no salinity and a 0.03 m depth.[51] The acoustic impedance was then determined from the measured density and speed of sound using the following equation

$$Z_s = SoS_s \times \rho_s \qquad (3)$$

where SoS_s is the average speed of sound through the sample and ρ_s is the average sample density.[38]

To measure acoustic attenuation (α_s), a sinusoidal tone burst of 20 cycles at a specific frequency (0.8, 1.2, or 1.6 MHz) was emitted. The received signals in the presence and absence of the sample were transformed to the Fourier domain and the max amplitude closest to the emitted frequency was measured. The attenuation was calculated using the following equation

$$\alpha_s = \frac{20}{h} \log_{10}\left(\frac{A_s}{A_w \times T_{ws}^2} \right) \qquad (4)$$

where h is the average sample thickness, A_s is the amplitude in the Fourier domain with the sample in place, and A_w is the amplitude in the Fourier domain with only water present.[44] T_{ws} accounts for the acoustic impedance mismatch between the water and sample using the following equation

$$T_{ws} = \frac{4 Z_w Z_s}{(Z_w + Z_s)^2} \qquad (5)$$

where Z_w is the acoustic impedance of water and Z_s is the measured sample acoustic impedance. The attenuation due to water is negligible and was not taken into account in the calculation.

Acoustic Impedance and Attenuation Modeling. Using the measured values, two models between the studied factors and the acoustic impedance and attenuation were determined using standard least squares in JMP. While the responses were originally collected in blocks to account for the variation that was possible across days of fabrication, preliminary analysis indicated no significant contribution to the response based on the day of fabrication, and therefore, the blocks were disregarded and least squares was used for analyses. Two samples (48 and 79) with high attenuation were removed from the modeling; the signals captured by the ultrasonic receiver through these samples during the acoustic impedance and attenuation characterizations could not be distinguished above the noise floor with no signal transmitted. The significant model terms were selected by maximizing the five-fold cross-validation with the fewest number of model terms while maintaining model hierarchy.

The final models were assessed with statistical tests and visually to confirm that no outlying or influential points skewed the model (assessed using leverage, Cook's distance, and studentized residuals), the errors were normally and independently distributed with a mean of zero and constant variance (assessed using the Shapiro–Wilk test), and the model demonstrated no significant lack of fit. The linear regression models were combined using the prediction profiler feature in JMP, which optimizes a desirability function to determine the factor settings to target specific response values. Two responses were targeted, including (1) the desired acoustic impedance value and (2) minimum or maximum attenuation.

To validate the final model, additional nine samples were fabricated that were not part of the original design of experiments. The model was used to predict how to fabricate samples with acoustic impedances of 1, 1.3, 1.6, 1.9, and 2.2 MRayls. Each of these impedances was targeted with a minimum and maximum attenuation, except for the 1 MRayl sample, which could only be fabricated using one formulation. The measured and predicted values from the model were compared to demonstrate the predictive strength of the combined models.

Demonstrating the Effect of Acoustic Impedance Matching. While there are various methods to demonstrate the effect of acoustic impedance matching on the output of underwater[52] and ultrasonic transducers,[53] these experiments typically measure the effect of an

added matching layer on the output of a specific transducer and use water as a coupling medium. To the authors' knowledge, a similar experiment has not been presented where, rather than changing a coupling layer, the sensor diaphragm material is varied. As the acoustic impedance and stiffness of the AIMS diaphragm are coupled, it would not be possible to make direct comparisons across AIMSs with different diaphragm materials because it cannot be guaranteed that they have the same sensitivity due to differences in micro-structure compressibility. Therefore, a simplified experiment was designed to demonstrate that precise control over the acoustic impedance of the diaphragm material will impact the transmitted acoustic intensity by measuring both (1) the acoustic velocity transmitted through various materials using a laser vibrometer and (2) the acoustic pressure through the AIMS with various diaphragm materials, both when excited with vibrations from base materials with different acoustic impedances.

Theoretically, it is well known that when an acoustic wave intersects perpendicularly at the boundary between two materials, the amplitude of the transmitted wave is determined by the corresponding acoustic transmission coefficient. The pressure change and molecular velocity of the incident wave must equal the sum of the components for the transmitted and reflected waves. From this requirement, it can be determined that the pressure transmission coefficient is

$$T_p = \frac{2 Z_2}{Z_1 + Z_2} \qquad (6)$$

while the molecular velocity transmission coefficient is

$$T_v = \frac{2 Z_1}{Z_1 + Z_2} \qquad (7)$$

where Z_1 is the acoustic impedance of the first medium and Z_2 is the acoustic impedance of the second medium.[2] As the velocity or pressure transmission coefficient increases, the amplitude of the velocity or pressure wave transmitted to the second material increases proportionally. The transmitted intensity or energy is a function of both the molecular velocity and the pressure. Therefore, to maximize energy transmission, it is desired to have velocity and pressure transmission coefficients near one, such that both the transmitted molecular velocity and pressure of the incident wave are maximized.

To demonstrate this effect with acoustic impedance-matched polymers fabricated for the AIMS, an acoustic phantom previously presented by the authors[54] was modified so that materials, such as wood and plastic, could be excited in place of a gelatin layer. The modified phantom, shown in Figure 3, contains a loudspeaker that excites a base material supported by a heavy aluminum plate and held fixed with magnets. The base materials, including aluminum ($Z \approx 17$ MRayls), bubinga wood ($Z \approx 1.65$ MRayls), high-density poly-ethylene (HDPE, $Z \approx 2.32$ MRayls), low-density polyethylene (LDPE, $Z \approx 1.9$ MRayls), red cedar wood ($Z \approx 0.74$ MRayls), red oak wood ($Z \approx 1.31$ MRayls), spruce wood ($Z \approx 0.52$ MRayls), and
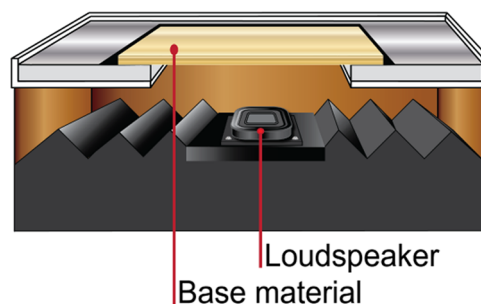

Figure 3. Modified acoustic phantom used for measuring the AIMS on varying materials. A base material is attached to a thick aluminum plate with a cutout using magnets such that white noise from the speaker can excite the base material.

steel ($Z \approx 45$ MRayls), were chosen to encompass a range of acoustic impedances, and all are approximately $120 \times 120 \times 3.5$ mm³. The loudspeaker emits white noise at a uniform level to excite each of these base materials.

To first provide a foundation for this experimental setup and validate that a relationship can be measured due to the acoustic impedance mismatch between air and the base material, the velocity at the surface of the base material was measured using a laser vibrometer (Polytec PDV-100), which has previously been used to estimate the acoustic velocity of different materials.[55] The setup is shown schematically in Figure S8a. The root-mean-square (RMS) voltage from the vibrometer was measured over a 5 s time window as the speaker excited the base material with white noise. Each base material was measured at five positions and repeated five times for a total of 25 measurements per base material. The goal of this experiment was to demonstrate that the experimental results agreed with theory, thereby providing validity for the experimental setup. A positive, increasing relationship was expected between the measured vibrometer output and the calculated velocity transmission coefficient $\left(T_{\text{v}-\text{air}-\text{bm}} = \frac{2Z_{\text{air}}}{Z_{\text{air}} + Z_{\text{bm}}}\right)$ between air ($Z \approx 0.0004$ MRayls) and the base material (Z_{bm}).

To then use this validated experimental setup to show that the acoustic impedance of the polymer diaphragm (Z_{dm}) has a measurable effect on the sensor output, the average AIMS voltage output was measured when constructed with three different diaphragm materials and excited by eight base materials, as shown in Figure S8b. The AIMS was held on the base material with a 50 g weight, excited with white noise, and the RMS signal was recorded for 10 s through an audio interface. Three AIMSs were assembled with diaphragms of (1) PDMS ($Z \approx 1.07$ MRayls), (2) polyurethane ($Z \approx 1.54$ MRayls), and (3) polyurethane with barium titanate dopant ($Z \approx 1.9$ MRayls) and measured five times on each base material. The output measured from the AIMS was normalized by the calculated pressure transmission coefficient from air to the base material $\left(T_{\text{p}-\text{air}-\text{bm}} = \frac{2Z_{\text{bm}}}{Z_{\text{air}} + Z_{\text{bm}}}\right)$, accounting for the impedance mismatch between air and the base material. A positive, increasing relationship was expected between the normalized AIMS output $\left(\frac{V_{\text{AIMS}}}{T_{\text{p}-\text{air}-\text{bm}}}\right)$ and the calculated pressure transmission coefficient $\left(T_{\text{p}-\text{bm}-\text{dm}} = \frac{2Z_{\text{dm}}}{Z_{\text{bm}} + Z_{\text{dm}}}\right)$ between the base and diaphragm materials. As the AIMS is responsive to acoustic pressure, this experiment only can quantify the relationship with the pressure transmission coefficient.

To demonstrate the other component of transmitted intensity, the velocity, the average velocity through various materials when placed on each base material was measured using a laser vibrometer, as shown in Figure S8c. The vibrometer measured the average velocity from four polymers (polyurethane with 32% silicon dioxide ($Z \approx 1.89$ MRayls), PDMS with 32% barium titanate ($Z \approx 1.32$ MRayls), polyurethane with 6.5% barium titanate ($Z \approx 1.67$ MRayls), polyurethane with 50% silicon dioxide ($Z \approx 2.16$ MRayls)) and eight other materials (aluminum, bubinga, HDPE, LDPE, red cedar, red oak, spruce, steel) when placed on the base material. As these measurements did not require AIMS fabrication, a larger selection of materials was used to generalize the findings. Steel and aluminum were removed as base materials for these experiments because they did not excite the polymer or material with an amplitude large enough to generate a measurable signal. Each polymer or material was measured five times on each base material. The RMS voltage from the vibrometer was measured over a 5 s time window as the speaker excited each of the polymers and materials on the base material with white noise. The vibration was measured at the center of each material using reflective tape. The output measured from the vibrometer was normalized by the calculated velocity transmission coefficient from air to the base material ($T_{\text{v}-\text{air}-\text{bm}}$), accounting for the impedance mismatch between air and the base material. A positive, increasing relationship was expected between the normalized

vibrometer output $\left(\frac{V_{\text{vib}}}{T_{\text{v}-\text{air}-\text{bm}}}\right)$ and the calculated velocity transmission coefficient $\left(T_{\text{v}-\text{bm}-\text{dm}} = \frac{2Z_{\text{bm}}}{Z_{\text{bm}} + Z_{\text{dm}}}\right)$ between the base and diaphragm materials, while a decreasing relationship was expected between the normalized vibrometer output and the pressure transmission coefficient ($T_{\text{p}-\text{bm}-\text{dm}}$). Together, the measured vibrometer and AIMS outputs for various polymers and base materials demonstrate that both the acoustic velocity and pressure, and therefore the intensity, are impacted by the acoustic impedance of the coupling material.

Voltage Response. To measure the sensitivity of the AIMS, the device was placed on a mini shaker (Brüel & Kjaer 4810) and held in a fixed position with a preload of 5 ± 0.1 N using a dynamic testing instrument (Instron Electropuls E1000), as shown in Figure S9. The mini shaker was excited with a continuous, 220 Hz sinusoidal vibration with peak-to-peak amplitudes ranging from 1 to 10 V in 1 V increments generated by a function generator (Tektronix AFG 3022B). A 220 Hz excitation was chosen because it represents a frequency that is central to the frequency band of body sounds.[56] The RMS voltages produced by the AIMS, a laser vibrometer (Polytec PDV-100), and a dynamic testing instrument load cell (Dynacell 2527 series 250 N) due to the mini shaker vibration were measured directly using an oscilloscope over a 5 s time window. The measured RMS voltage from the laser vibrometer and load cell were converted to millimeters per second and newtons using the reported scaling factors of 5 mm/s/V and 10 N/V, respectively. The ratio of the RMS AIMS voltage and the RMS voltage from the load cell was calculated to determine the sensitivity in terms of V/N. Four AIMSs were measured three times each, and the responses were averaged for each device. An AIMS with an uncharged FEP layer was also measured as a control. The signal-to-noise ratios (SNRs) of the AIMSs and vibromter were also measured at 220 Hz by calculating, in decibels, the average ratio of the RMS voltage when the vibrational force from the shaker was applied and the RMS voltage when no force was applied.

To understand how the sensor behaves when compressed with increasing preload forces, but the same excitation, the AIMS was placed on the acoustic phantom, described in the "Demonstrating the Effect of Acoustic Impedance Matching" section, with a HDPE sheet and excited with a 350 Hz tone from a speaker. A 350 Hz tone was used in this case as it was found to propagate through the HDPE layer better than a 220 Hz tone. The sensor was held fixed on the phantom using the dynamic test instrument, and by varying the fixed position of the dynamic test instrument, the preload applied to the sensor was varied. The RMS voltage output from three sensors was measured three times directly from an oscilloscope over a 20 ms time window at 26 randomly selected preloads between 2 and 15 N and normalized by the applied load amplitude, as measured by the dynamic test instrument load cell.

Stability. To understand the stability of the AIMS over time, the AIMS was placed on the mini shaker the day it was fabricated, held in place with a 200 g weight, and excited with a 220 Hz, 4 V peak-to-peak signal from the function generator for 7 continuous days. The RMS voltage recorded by the oscilloscope over a 5 s time window was measured three times and averaged at randomly selected intervals within the 7 days. This process was repeated with four AIMSs and a control AIMS with an uncharged FEP layer. The stability of the AIMS at elevated temperatures was assessed by measuring the sensitivity using the same procedure described in the "Voltage Response" section immediately before and after the AIMS was placed on a hot plate at approximately 80 °C for 1 h. The temperature stability of the AIMS was measured for three sensors.

Frequency Response. The frequency response of the AIMS was measured using both a mini shaker and an acoustic phantom that mimics the characteristics of the human body. Using the mini shaker, the AIMS was excited with sinusoidal vibrations of 23 frequencies evenly spaced from 70 to 585 Hz, while the dynamic testing instrument held the AIMS in a fixed position with a preload of 5 ± 0.1 N. The lower and upper frequencies were set by the limitations of the
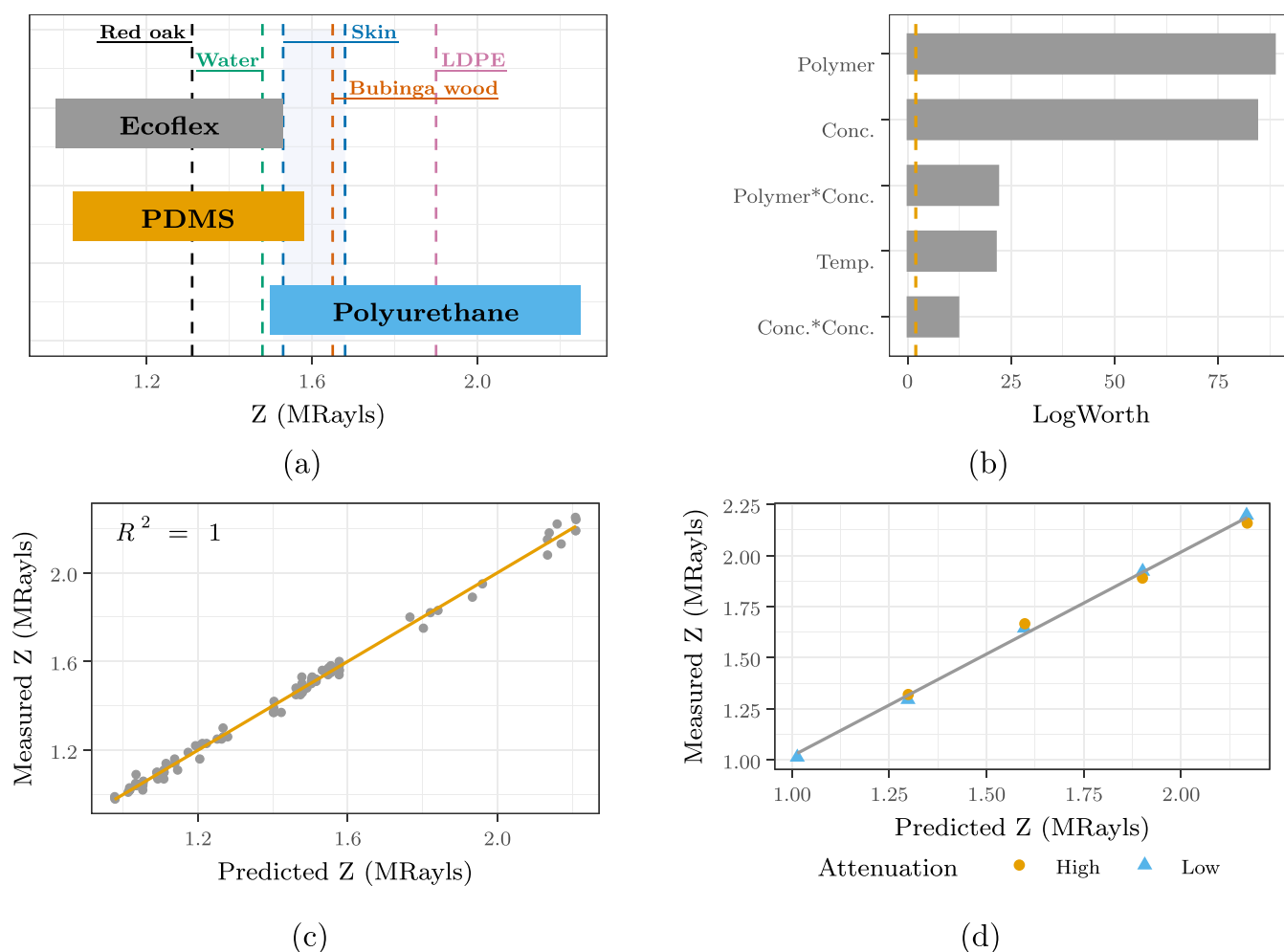
Figure 4. Results from the design of experiments to understand the acoustic impedance of polymers; (a) range of measured Z values for each of the polymers included (Ecoflex, PDMS, polyurethane), (b) significant effects determined for predicting Z ranked by their LogWorth, (c) predicted versus measured values of Z, and (d) predicted versus measured values of nine samples used for validation with five impedance values and low or high attenuation.

mini shaker used and chosen to align with the frequencies tested using the acoustic phantom setup. The amplitude of the shaker vibration was adjusted such that the load applied to the AIMS was within 0.4 ± 0.01 N for all frequencies. The RMS voltage generated by the AIMS for each frequency was measured through the oscilloscope over a 5 s time window and converted to decibels. The process was repeated for a total of three AIMSs, and the responses were averaged using the RMS average in the linear scale.

To measure the frequency response in conditions more similar to body sound monitoring and to compare to existing stethoscopes, the AIMS was placed at the center of an acoustic phantom, held with a 200 g weight, and excited with a logarithmically swept sine sweep, as previously described by the authors.[54] As a summary, room EQ wizard (REW) software[57] generated a sine sweep and analyzed the response of the AIMS using the methods outlined by Müller.[58] The sine sweep conditions were set to a frequency range between 20 and 1000 Hz, a length of 1 Ms, −12 dBFS RMS signal level, a 44.1 kHz sample rate, and a single repetition. The sine sweep generated by REW was sent from the computer to the acoustic phantom's driver amplifier, and the AIMS output was sent through an audio interface (Focusrite Scarlett 2i2) with the gain adjusted to record a clear signal. The acoustic phantom, which is also described and validated in ref 54, used a loudspeaker to excite a 10 mm thick gelatin layer supported by a grid and was kept at a uniform volume to excite the device under test. The same process was used to measure the frequency responses of six other devices, shown in Figure S10, including two commercial

stethoscopes (Thinklabs One, Sonavi Labs Feelix), an accelerometer (PCB Piezotronics 352C66), a flexible piezoelectric film (TE Connectivity SDT1 Piezo Film Sensor), and a vibrometer (Polytec PDV-100) for comparison. The vibrometer response was measured 10 times to average over a larger area, while all other devices were measured 5 times. The individual measurements for each device were averaged using the RMS average in the linear scale. For the vibrometer specifically, the response was measured on a piece of reflective tape placed at the center of the acoustic phantom. The accelerometer was held fixed with an adhesive, while all other devices were held using a 200 g weight in the same manner as the AIMS.

Noise Rejection and Signal Fidelity. To quantify how well the AIMS captures the signal of interest and rejects airborne noise in conditions that mimic monitoring from the human body, but also allow for precise control over the acoustic environment, a process previously presented by McLane et al.[8] was used. In short, the signal fidelity and noise robustness were measured in a sound booth, shown schematically in Figure S11, with simulated noise environments from 60 to 90 dB SPL while lung sounds, representing both normal and abnormal physiologies, were played from the same acoustic phantom used for frequency response characterization. The ambient noise consisted of stationary sounds (white, pink, blue, and Brownian noise), as well as nonstationary sounds (hospital ICU noise, hospital corridor noise, pulse monitor sounds, ambulance noise, multispeaker babble noise, baby cry, street noise, chirping birds, air conditioner, announcements, appliances (washer/dryer), car noise, copy machine,

door shutting, and eating) found in the BBC and NoiseX-92 databases.[59,60] The sounds were broadcast from two speakers (Yamaha HS8) such that the measured noise near the acoustic phantom averaged to sound levels ranging from 60 to 90 dBC SPL at 5 dB increments. The amplitudes of the ambient noise signals were adjusted with a multiplicative factor until the 75th percentile of the measured sound levels was within ±2.5 dBC of the desired ambient sound level, as measured by a sound level meter (Martel Electronics 322). The ambient sounds were randomly combined with a selection of 50 lung sounds, each 10 s in length, to be played from the acoustic phantom. The lung sounds were played at a fixed level across all recordings. Ten abnormal and 10 control breath sounds were selected from a teaching dataset,[61] with additional 10 normal breath sounds, 10 breath sounds with crackles, and 10 breath sounds with wheezing from patients of broad age ranges collected in well-controlled clinical environments included.[62]

The signal fidelity and noise robustness of the AIMS were quantified by comparing the lung sound recorded by the AIMS (y) against the reference lung sound signal driving the acoustic phantom (x) and the background noise recorded by a calibrated microphone positioned near the acoustic phantom (d). The AIMS was recorded using a Zoom H6 recorder at an 8 kHz sampling rate and low-pass filtered at 500 Hz to match the frequency content of typical stethoscopes. As described in greater detail by McLane et al.,[8] two existing speech-based objective quality metrics were chosen to quantify the similarity between the reference lung sound (x) and AIMS signals (y) and the amount of dissimilarity between the ambient (d) and AIMS signals (y): normalized covariance measure (NCM) and magnitude squared coherence (MSC).[63] The overall quality metric calculates the geometric mean of the NCM and MSC metrics for various window lengths and signal pairs to quantify (1) how well the recorded AIMS signal (y) represents the original lung sounds (x)($SNR_{lungsounds}$) and (2) how much noise (d) is present in the recorded AIMS signal (y) (SNR_{noise}). The final metric, SNR_{est}, is then calculated by subtracting SNR_{noise} from $SNR_{lungsounds}$.

The AIMS was measured both directly on the acoustic phantom and on the acoustic phantom with a thin cotton fabric on the gelatin layer to understand how the device performance changed when placed directly on the skin or on a thin item of clothing. For comparison purposes, the same process to characterize the noise rejection and signal fidelity of the AIMS was repeated for two commercial stethoscopes (Thinklabs One, Sonavi Labs Feelix), an accelerometer (PCB Piezotronics 352C66), a flexible piezoelectric film (TE Connectivity SDT1 Piezo Film Sensor), and a vibrometer (Polytec PDV-100).

Use on the Body. To determine how well the AIMS captures body sounds on a real subject, the device was placed on a healthy adult male using medical adhesive on the tricuspid region for heart sounds and on the right axilla for lung sounds in a quiet office setting. The output of the AIMS was captured with an audio interface (Focusrite Scarlett 2i2) and recorded in Audacity at a sampling rate of 4 kHz. The lung and heart sound recordings were processed with low-pass (400 Hz cutoff and 24 dB roll-off) and high-pass (20 Hz cutoff and 48 dB roll-off) filters to match the frequency content of typical stethoscopes[64] and to capture the primary frequency content of lung sounds below 300 Hz.[65]

RESULTS AND DISCUSSION

Acoustic Impedance and Attenuation Models. The I-optimal design of experiments involved fabricating and characterizing Ecoflex, PDMS, and polyurethane samples with a variety of types and concentrations of added nanoparticles. As shown in Figure 4a, a range of acoustic impedances from approximately 1 to 2.2 MRayls were measured, and with the proper choice of polymer and added particles, the polymers can be fabricated to match materials such as water ($Z \approx 1.48$ MRayls[6]) and skin ($Z \approx 1.53-1.68$ MRayls[5]), as well as various woods[66] and plastics[45] that have

acoustic impedances within this range. With the chosen factor levels, Ecoflex, PDMS, and polyurethane demonstrated acoustic impedance ranges of 0.98−1.53, 1.02−1.58, and 1.5−2.25 MRayls, respectively.

Within these acoustic impedance ranges, the developed statistical model predicts the necessary fabrication parameters to match a specific target value. As shown in Figure 4b, factors that were significant to predict the acoustic impedance included polymer type, dopant concentration, an interaction between polymer type and dopant concentration, temperature, and the second power of concentration. On the plot, a greater logworth, which is equal to the negative log of the p-value, indicates a greater effect on the response. Figure 4c shows that the predicted and measured data fit extremely well ($R^2 = 1$) along the diagonal line, which indicates the adequacy of the model to predict acoustic impedances within this range accurately, given the fabrication conditions. To match skin specifically, which has an acoustic impedance in the range of 1.53−1.68 MRayls, there are several polymer formulations that could be used: PDMS with 50% dopant ($Z \approx 1.58$ MRayls), Ecoflex with 50% dopant ($Z \approx 1.53$ MRayls), and polyurethane with 10.6% dopant ($Z \approx 1.6$ MRayls). Diagnostic plots for the acoustic impedance model are provided in Figure S12.

A similar model was obtained for the acoustic attenuation, and it was determined that dopant concentration, frequency, polymer type, an interaction between polymer type, dopant density, and dopant concentration, and the second power of temperature are the most significant effects. Due to the uncertainties that arise in the measurement method, the attenuation model had a lower fit ($R^2 = 0.78$) than the acoustic impedance model but was able to inform factors that will maximize or minimize the attenuation. As the main focus of the paper is on acoustic impedance matching, further details on the attenuation model are provided in the Supporting Information (Figures S13 and S14).

To validate the combined effects of the acoustic impedance and attenuation models, additional nine samples that were not a part of the original design of experiments were fabricated. The goal was to fabricate samples with acoustic impedances of 1, 1.3, 1.6, 1.9, and 2.2 MRayls each with a lower and higher attenuation, except for the sample with an acoustic impedance of 1 MRayls which could only be fabricated using one formulation. As shown in Figure 4d, the predicted and measured impedance have high agreement with an average percent error of 1.39%, a difference of only about 0.02 MRayls. The model also predicted how to fabricate the polymers with a lower and higher attenuation; on average, the lower attenuation samples had a 37% lower attenuation than the high attenuation samples. In the case of continuing to match the acoustic impedance of skin while minimizing attenuation, a lower dopant concentration is preferred based on the model. Therefore, polyurethane is an optimal choice, specifically with a lower dopant density. For the sensor optimized for body sound monitoring, a polyurethane diaphragm was used as its measured acoustic impedance ($Z \approx 1.54$ MRayls) is well within the range of the body ($Z \approx 1.53-1.68$ MRayls), and it would demonstrate minimal attenuation without added particles. Overall, the experiments here demonstrate the use of the developed statistical model to fabricate one of three polymers as a polymer diaphragm to match the desired acoustic impedance value with minimum attenuation. Compared to existing work on impedance matching, this
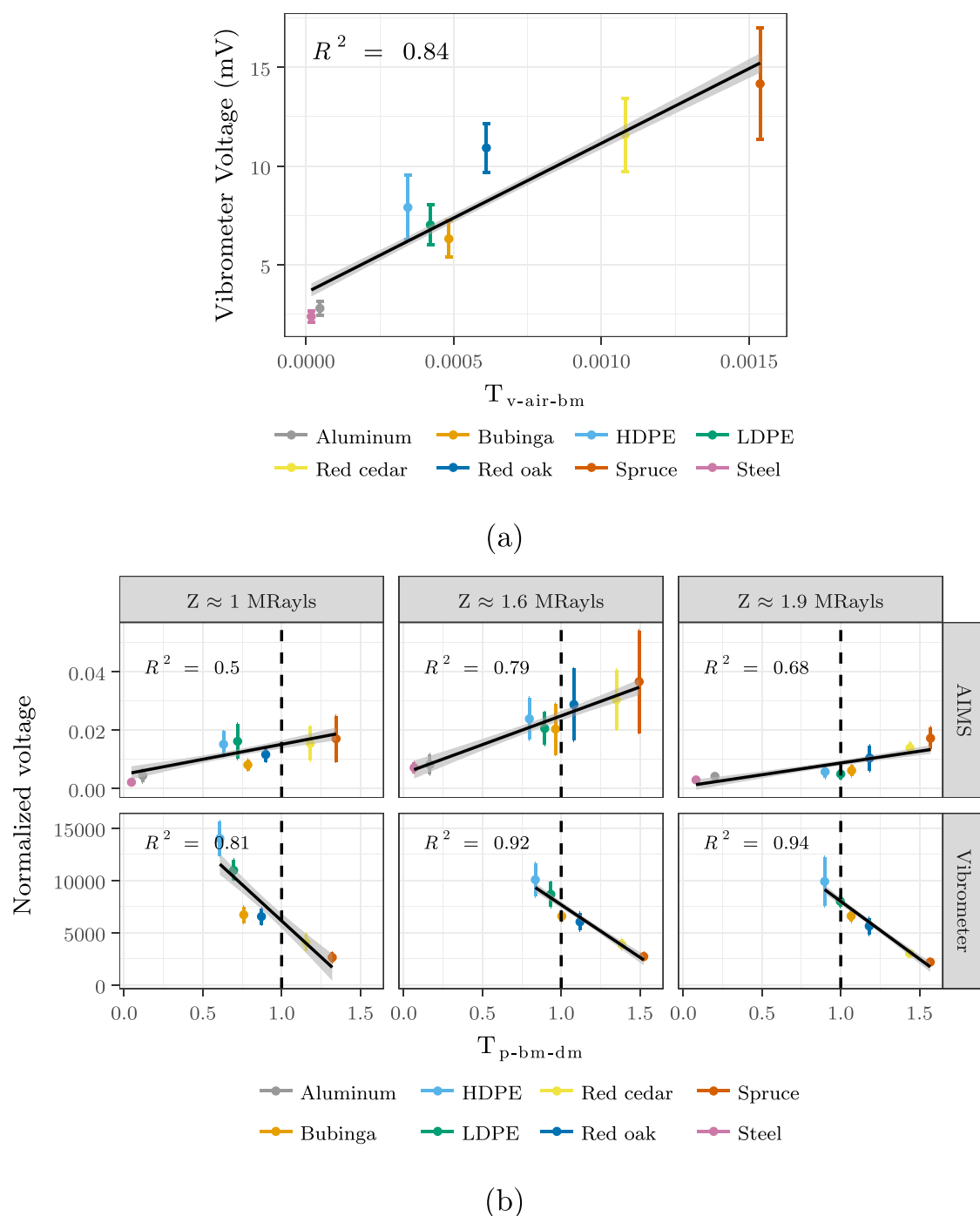
(a)

(b)

Figure 5. Results of the experiments to show that the acoustic impedance of the AIMS diaphragm has a measurable effect on both the transmitted velocity and pressure; (a) vibrometer voltage measured from a base material with respect to the velocity transmission coefficient from air to the base material and (b) AIMS and vibrometer voltage measured with respect to the pressure transmission coefficient from the base to diaphragm materials.

model allows broader generalizations and includes interactions between factors.

Acoustic Impedance Matching Effect. Figure 5a shows the average vibrometer voltage measured against the calculated velocity transmission coefficient for air to eight different base materials. As theory predicts, there is a strong, increasing linear relationship ($R^2 = 0.84$) between the velocity transmission coefficient and vibrometer voltage. The highest velocity is measured for the material with lowest acoustic impedance (spruce), and the lowest velocity is measured for the material

with the highest acoustic impedance (steel). As a simplified experiment, the linear trend does have some slight deviations, likely due to differences in acoustic attenuation or variations in the wood materials due to grain orientation. However, the results indicate that the general trend between the velocity transmission coefficient and velocity is indeed measurable using the laser vibrometer for sound traveling from air through the base material.

Figure 5b shows the normalized voltage measured from the AIMS and vibrometer when polymers with acoustic impedance

of approximately 1, 1.6, and 1.9 MRayls are placed on each base material with respect to the calculated pressure transmission coefficient from the base to diaphragm materials. The AIMS demonstrates an increasing relationship with pressure transmission coefficient (average $R^2 = 0.66$), while the vibrometer demonstrates a decreasing relationship (average $R^2 = 0.89$). As expected, when the transmission coefficient is equal to approximately one, there is a balance between maximizing both the vibrometer and AIMS output or the transmitted velocity and pressure. These experiments demonstrate that the acoustic impedance of the AIMS diaphragm has a measurable effect on both the transmitted velocity and pressure. By more closely matching the acoustic impedance of the medium being monitored, the transmitted pressure and velocity will both be maximized. The results of measuring additional materials with the laser vibrometer on the base materials are provided in Figure S15.

Sensitivity. Figure 6 shows the output voltage measured from four AIMSs (all fabricated following the same procedure)
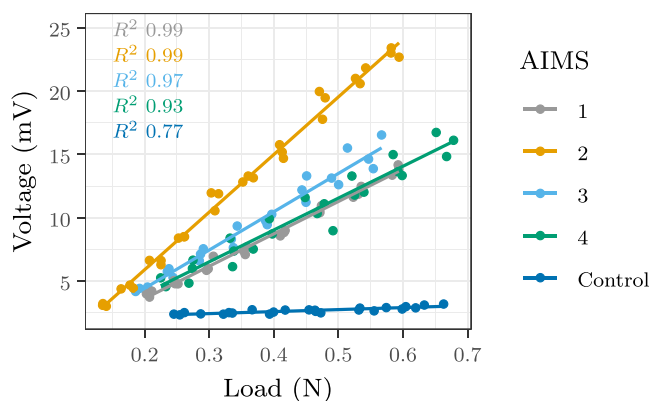

Figure 6. RMS voltage measured from four AIMSs and a control as the applied load increases.

and a control with an uncharged FEP layer as the applied load increases, but the preload is fixed at approximately 5 N. All AIMSs show a linear response when fitted individually with R^2 values of 0.99, 0.99, 0.97, and 0.93, but with varying slopes that indicate the sensitivities. The average sensitivities are 21.3, 34.0, 25.3, and 22.6 mV/N for AIMSs one through four, respectively. The varying sensitivities for each AIMS are likely due to fabricating the sensor by hand, which leads to variations in the charge stored within the electret film. The average AIMS sensitivity is approximately 4 times greater than the sensitivity of the control AIMS, 6.4 mV/N, and also comparable to the vibrometer sensitivity, 22.9 mV/N, measured using the same technique. The average SNRs for the AIMS and vibrometer were 4.48 and 5.27 dB, respectively. Together, these results indicate that the AIMS is highly sensitive with a linear response that is comparable to a laser vibrometer.

Figure 7 shows the average responses from three AIMSs normalized by the applied load amplitude with various preloads applied. As the preload increases, there is a decreasing, linear trend in the average AIMS response. This decreasing trend was expected because as the polymer diaphragm is compressed with increasing preloads, the microstructures are deformed and require a greater vibrational amplitude to compress. As such, the voltage output would decrease for the same applied load amplitude. A typical stethoscope is typically held to the body with approximately 3
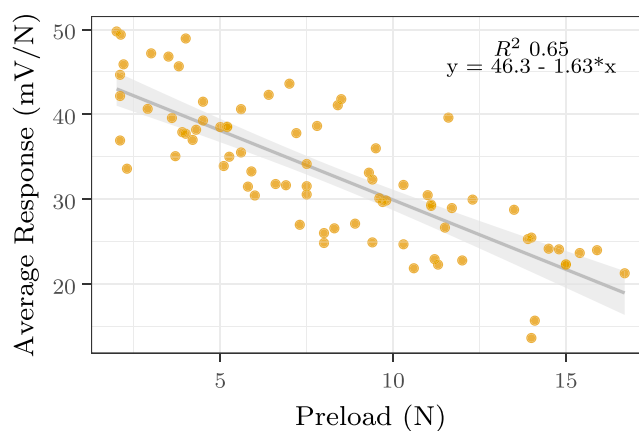

Figure 7. Average response measured from three AIMSs placed on the acoustic phantom with an HDPE layer and excited with a 350 Hz tone as the applied preload is increased.

N of force.[7] In this range, the AIMS remains highly sensitive to the acoustic vibration and the decrease in output with increasing preload could be compensated by applying gain.

Stability. As shown in Figure 8a, the AIMS demonstrates a voltage output that exponentially decays initially before reaching a stable output after two to 3 days of excitation. The dashed line in the figure indicates the voltage output of the control AIMS with an uncharged FEP layer. After 7 days of continuous excitation, all AIMSs with a charged FEP layer outperform the control, which confirms that charge is still held within the FEP film. The initial decay in output was expected as there are various internal and external phenomena, such as ion deposition, Ohmic conduction, and excess charge diffusion, that lead to charge redistribution and compensation in electret films.[67] The specific charging conditions used to fabricate the AIMS were not optimized, but there are multiple approaches, including the charging method, annealing the sample following charging, and charging the sample multiple times, that could be used to improve the charge storage and stability further.[67] Beyond 7 days of continuous excitation, AIMSs have been observed to capture usable acoustic recordings 1.5 years after their initial fabrication when stored at room temperature.

Figure 8b shows the measured sensitivities of three AIMSs immediately before and after heating on a hot plate. The Wilcoxon test indicates that two out of the three AIMSs (1, 2) measured had no significant difference (p-value >0.05) in average sensitivity before and after heating. The AIMS (3) that showed a significant difference was fabricated on the same day of testing, while the other two had been fabricated 14 days prior. The sensitivity change for AIMS 3 likely indicates that the heating process accelerated the exponential charge decay that was detected in the continuous excitation measurements. Overall, these results indicate that the AIMS (1) has a stable response after an initial decay and (2) is robust to the temperature changes found in typical body sound monitoring.

Frequency Response. The frequency response of the AIMS measured with the mini shaker and acoustic phantom is shown in Figure 9a. Both methods indicate that the AIMS has a fairly flat frequency response between 70 and 500 Hz, a frequency range critical for capturing body sounds. The frequency content of lung sounds is generally concentrated within 100−400 Hz and with a median frequency of approximately 200 Hz with slight variations based on the disease state.[68] The frequency response measured from the
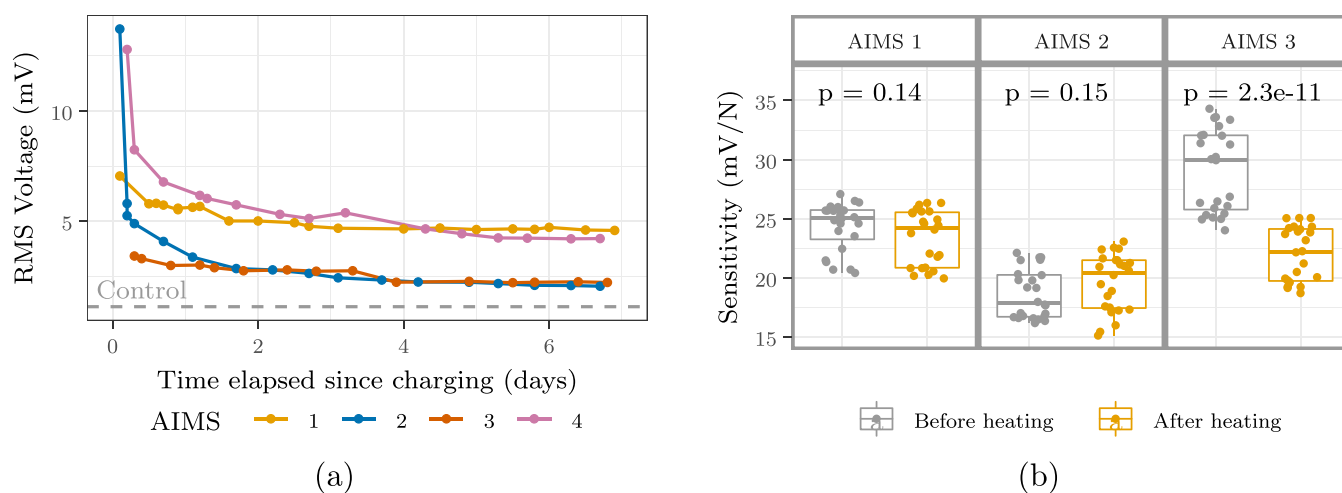
(a)　　　　　　　　　　　　　　　　(b)

Figure 8. Stability of the AIMS (a) when measured across 7 days of continuous excitation and (b) before and after heating.
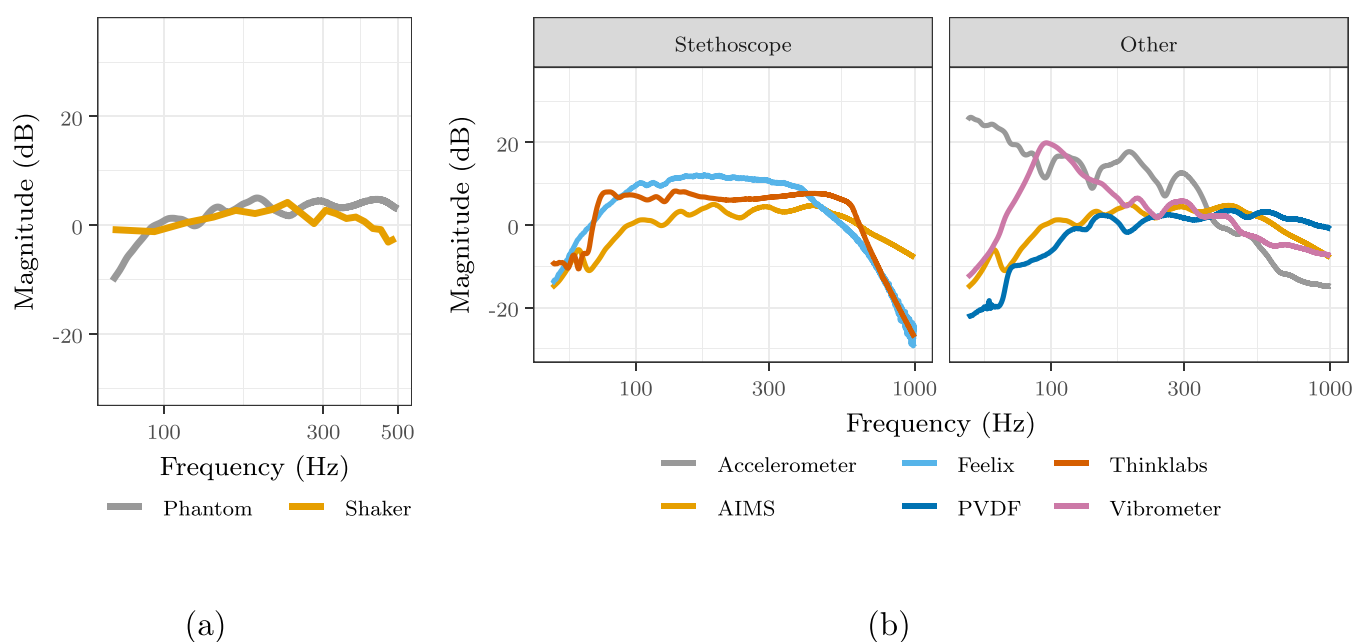

(a)　　　　　　　　　　　　　　　　(b)

Figure 9. Frequency response of the AIMS when (a) measured using an acoustic phantom and a mini shaker and (b) compared to several other devices.

shaker has a spread of 7.3 dB, while the acoustic phantom has a spread of 15.4 dB for the full frequency range measured and of 5.1 dB above 100 Hz. Visually, the responses measured using each methods are similar but diverge at lower (<100 Hz) and higher frequencies (>400 Hz). The responses have average and maximum differences of 3.3 and 9.4 dB, respectively. The discrepancies that exist between the measurement methods could be a result of how the sensor is held fixed on the shaker or phantom.

The AIMS response is comparable with the responses from commercially available stethoscopes, as shown in Figure 9b on the left. These measured responses, as well as stethoscope responses in the literature, show a peak of 200 Hz and 40−50 dB roll-off between 200 and 1000 Hz.[69] The AIMS response is comparable to the two commercial stethoscopes measured, the Feelix and the Thinklabs, with correlations of 0.83 and 0.86, respectively, but with the ability to capture higher frequencies. Though the AIMS has a higher magnitude response in the

higher frequencies comparatively, this can be easily mitigated in practice using simple bandpass filtering.

In Figure 9b on the right, the frequency responses of several other devices capable of monitoring body sound vibrations are shown for comparison purposes. The vibrometer and accelerometer show frequency responses with much more pronounced peaks, while the PVDF film demonstrates a similar response to the AIMS with more low-frequency peaks. The vibrometer, accelerometer, and PVDF film have correlations of 0.65, 0.64, and 0.19 with the Thinklabs and 0.78, 0.79, and 0.11 with the Feelix. Overall, the flat frequency response of the AIMS and its similarity to commercially available stethoscope demonstrate that it has the characteristics necessary to capture critical frequency information from body sounds with comparable or better accuracy than other available sensing methods.

Noise Rejection and Signal Fidelity. Figure 10 illustrates the performance of six sensors (AIMS, Feelix, Thinklabs, accelerometer, PVDF film, and vibrometer) when excited with
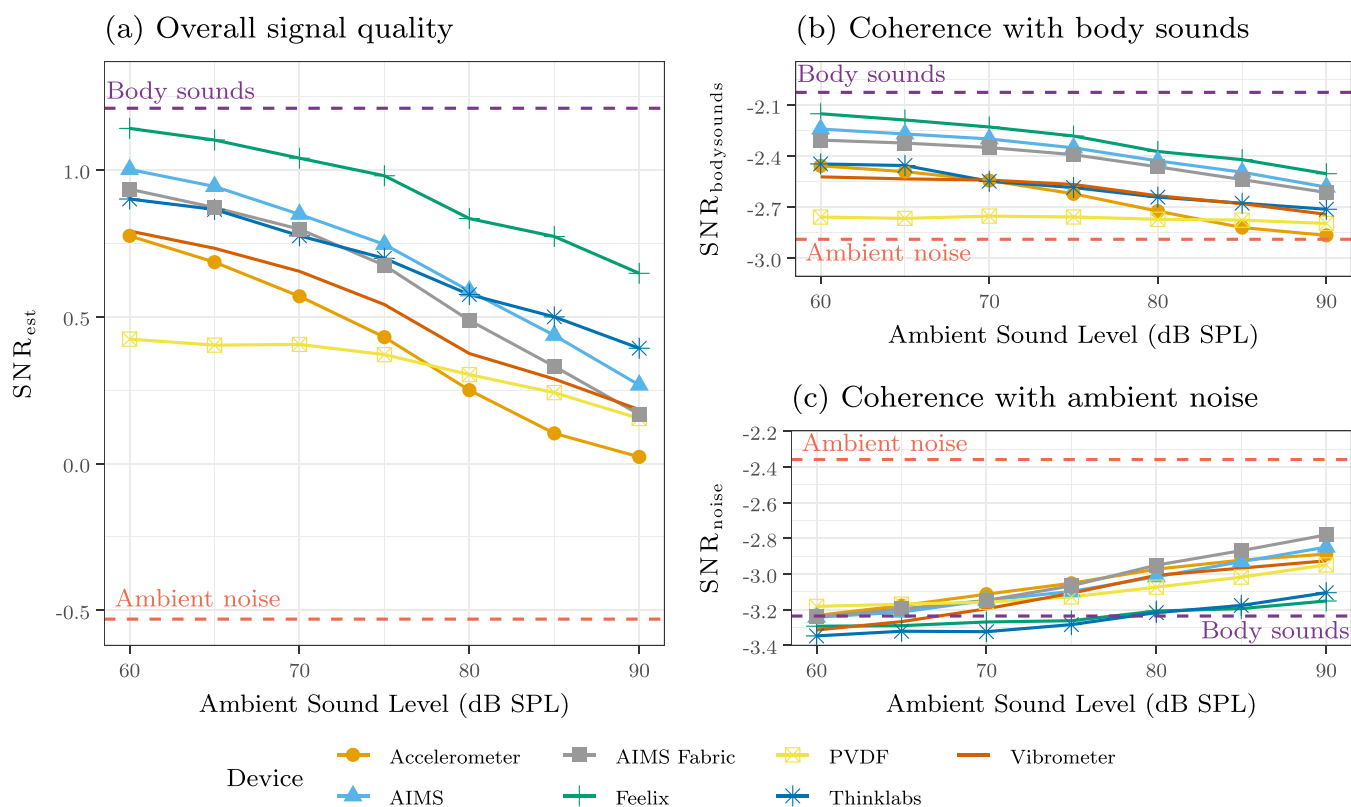
Figure 10. Illustration of the sound-preservation and noise-rejecting ability of the AIMS compared to several devices with regards to the calculated (a) overall signal quality, (b) coherence with body sounds, and (c) coherence with ambient noise.

body sounds from the acoustic phantom at varying simulated noise levels, with 60 dBC SPL representing a well-controlled environment that would be typical in clinical work and 90 dBC SPL representing an extremely loud and challenging environment that would represent the upper limit of noise in emergency or ambulatory settings or community clinics in low- and middle-income countries. High values of the SNR_{est} metric represent increased body sound signal fidelity and reduced noise sensitivity, while low values reflect decreased signal quality and increased noise contamination. The dashed lines labeled "body sounds" and "ambient noise" indicate the metrics for copies of the body sound signal driving the acoustic phantom and the ambient noise measured by a calibrated microphone, respectively. These dashed lines demonstrate the bounds of expected values from the device capturing purely body sounds or purely ambient noise.

Comparing each device's coherence with body sounds, shown in Figure 10b, the Feelix and the AIMS show the highest coherence with body sounds that decays linearly as the ambient sound level increases. The Feelix likely has improved coherence with body sounds due to its use of multiple microphones across the surface. The Feelix and the AIMS slightly outperform the accelerometer, Thinklabs, and vibrometer. Above 75 dB, the accelerometer demonstrates a steeper decrease in the coherence compared to the Thinklabs and accelerometer. The PVDF sensor demonstrates the lowest coherence, likely due to its low sensitivity in comparison to the other devices. The AIMS measured on a thin fabric layer does demonstrate a decrease in the coherence with body sounds but maintains a higher coherence than the Thinklabs. The average $SNR_{bodysounds}$ is significantly different for all devices at 75 dB (p-value <0.05), except for the Thinklabs and accelerometer.

With regards to the coherence with ambient noise, shown in Figure 10c, the Thinklabs and Feelix demonstrate the lowest coherence across all sound levels. This is expected as these devices both use onboard noise cancellation. A low coherence with the ambient noise from pronounced filtering likely contributes to the lower coherence with the body sounds in the Thinklabs because it is removing some of the signal of interest, as depicted in previous results.[8] It is observed that the vibrometer demonstrates an increase in coherence with ambient sound levels. As the vibrometer is theoretically insensitive to airborne noise, this indicates that as the sound level increases, the surface of the phantom conducts airborne noise, which is subsequently captured by the various contact sensors. This occurrence would not similarly affect the Feelix and Thinklabs performance because of the noise suppression schemes used. At 75 dB, none of the devices demonstrate a significant difference (p-value >0.05) in the coherence with noise compared to the AIMS. This indicates that the AIMS has comparable performance with regards to noise rejection due to its use of contact sensing and the impedance-matched diaphragm. In particular, no significant difference between the AIMS and vibrometer confirms that the AIMS has low sensitivity to airborne noise, as the vibrometer should be fully isolated from any airborne noise vibrations.

The overall combined metric SNR_{est}, shown in Figure 10a, indicates that Feelix has the best overall performance due to its high coherence with body sounds and low coherence with ambient noise, a product of the optimized multiband spectral subtraction scheme. The AIMS has the second best performance below 80 dB but is outperformed by the Thinklabs above 80 dB. This is likely a consequence of the onboard noise rejection in the Thinklabs removing added noise that conducts
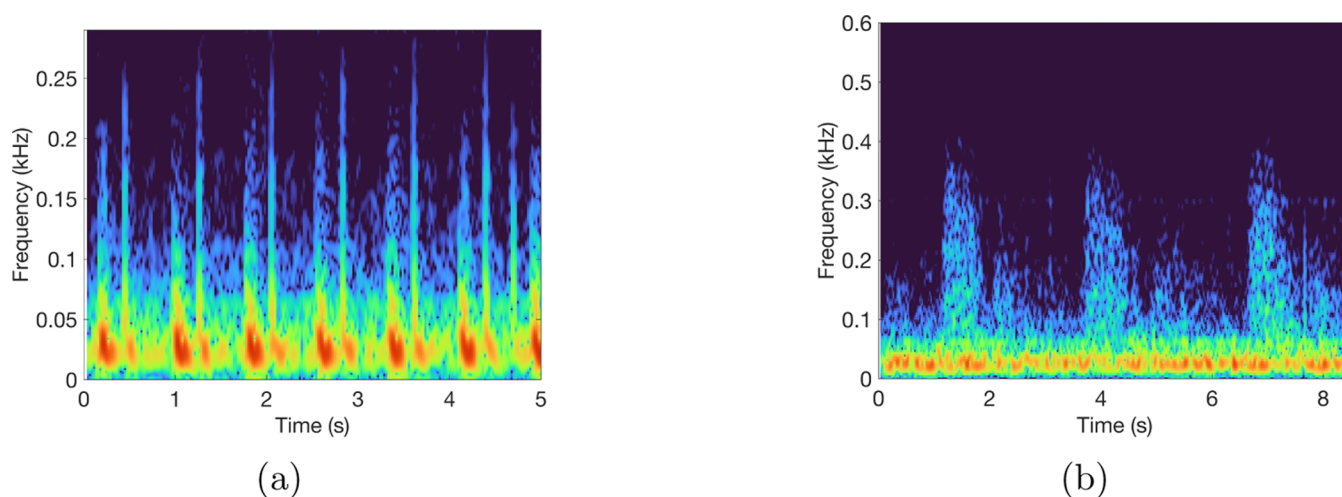
Figure 11. Spectrograms from recording a healthy male subject (a) on the tricuspid region, which captures heart sounds more prominently and (b) on the right axilla, which captures lung sounds more prominently.

through the phantom coupling layer. The AIMS measured with a fabric layer maintains comparable performance to the Thinklabs below 75 dB and is not significantly different from the AIMS without a fabric layer at 75 dB (p-value >0.05). The vibrometer demonstrates a curve that has an overall similar trend to the AIMS, but the SNR_{est} values are shifted downward by approximately 0.25, possibly due to only capturing vibrations at a small point on the phantom. The accelerometer and PVDF film show the lowest overall performance, with the accelerometer coherence decreasing rapidly above 80 dB due to poor pickup of body sounds. At 75 dB, the Feelix and the PVDF film are significantly different from all devices (p-value <0.05), the AIMS is not significantly different from the AIMS with a fabric layer (p-value >0.05), and the accelerometer, Thinklabs, and vibrometer are not significantly different (p-value >0.05).

Overall, the results demonstrate that the AIMS has performance that falls between two commercially available, state-of-the-art electronic stethoscopes with computationally intensive onboard noise cancellation. The AIMS outperforms other passive contact sensing devices, including a vibrometer, poly(vinylidene difluoride) (PVDF) film, and accelerometer. Though there is a slight decrease in the AIMS performance above 85 dB, there remains significant promise for the utility of the AIMS in noisy, ambulatory environments: while peak levels in challenging clinical environments may exceed 85 dB, these levels are generally transient in nature and not sustained for long periods of time as was done in this experimental setup.[70]

Use on the Body. Figure 11 shows the spectrograms of the recorded lung and heart sounds by the AIMS when placed on a healthy adult male. The beating of the heart is clearly visible in Figure 11a when the sensor is placed the tricuspid region, while the inhale and exhale pattern from the subject breathing is visible in Figure 11b when the sensor is placed on the right axilla. The audio recordings used to create the spectrograms are available in the Supporting Information. While a larger clinical study would be necessary to validate the use of the AIMS on a larger population of subjects, the recordings demonstrate the ability of the device to clearly capture lung and heart sounds.

Discussion. The results of this work have led to several outcomes: (1) the design of a new acoustic sensor with a single layer that can be tuned to specifically match the acoustic

impedances of multiple materials, (2) a validated, statistical model that can precisely predict the correct fabrication conditions for three polymers to match acoustic impedances in the range of 1−2.2 MRayls, (3) the use of this model to fabricate AIMS with varying acoustic impedances that are used to demonstrate the diaphragm material has a measurable effect on the transmitted velocity and pressure, and (4) characterization of the sensor, optimized specifically for body sound monitoring, with comparisons against commercially available stethoscopes. Compared to existing research, the AIMS makes use of a single layer to act as both the acoustic impedance matching and transduction mechanisms, uses a simple fabrication process, and does not include rigid components.

During a strong preliminary study of the sensor design and demonstration of its performance capabilities, it is important to note the following when considering the results of the experiments described in this paper: (1) the combined effect of acoustic impedance and microstructure stiffness was not explored in the sensor design; (2) the sensor was specifically optimized for body sound monitoring in this study, but it would be straightforward to tailor the diaphragm to match another acoustic impedance using the developed statistical model; and (3) susceptibility to motion artifacts was not considered in this study. In the future, the design of the AIMS could be expanded to better optimize the stability and improve the form factor to a truly wearable design with onboard battery power and wireless data transmission. A number of follow-up studies would also need to be conducted to validate and optimize the AIMS for use on a larger population and in clinical practice. Although a number of challenges remain, it is envisioned that this sensor could provide an improved method for monitoring body sounds.

■ CONCLUSIONS

In summary, a design for an electrostatic acoustic sensor with a diaphragm fabricated to specifically match the medium of interest has been presented and specifically characterized for body sound monitoring. Using a design of experiments approach, a model was developed that can accurately predict how to fabricate the sensor's polymer diaphragm with a specific acoustic impedance in the range of 1−2.2 MRayls to match materials such as water, skin, and wood. The core novelty of

the transducer design is the capability to use this model to design an impedance-matched layer that also acts as the transduction layer, minimizing the energy reflected away from the transducer without the use of multiple matching layers. For body sound monitoring specifically, an added benefit of this approach is that the diaphragm that closely matches the acoustic impedance of skin passively eliminates airborne energy by reflecting it at the air−transducer interface. This passive and highly effective noise suppression mechanism effectively implements noise cancellation, without computationally heavy signal processing and noise cancellation algorithms, such that the sensor demonstrates comparable noise rejection to a laser vibrometer that is insensitive to airborne noise.

Through various acoustic characterizations, the sensor was demonstrated to be highly sensitive to the body sound of interest and less sensitive to airborne noise. In fact, the proposed sensor had comparable coherence with body sounds to a commercially available electronic stethoscope with onboard noise cancellation algorithms. The transducer was also demonstrated to have a similar sensitivity to a commercially available vibrometer, be robust over time and at elevated temperatures, and have a frequency response comparable to typical stethoscopes. Due to its thin design with flexible materials and ability to capture clear body sounds in noisy environments, the transducer would be well-equipped for long-term, wearable body sound monitoring. While this study focused on the transducer's capabilities for body sound monitoring, its characteristics could make it well-equipped for monitoring other mediums as well, such as underwater or musical instrument pickup.

ASSOCIATED CONTENT

Supporting Information

The Supporting Information is available free of charge at https://pubs.acs.org/doi/10.1021/acsabm.3c00359.

Experimental details, materials, and methods, including photographs of experimental setup (PDF)

Lung and heart sound recordings (ZIP)

AUTHOR INFORMATION

Corresponding Author

James E. West − *Department of Electrical and Computer Engineering, Johns Hopkins University, Baltimore, Maryland 21218, United States*; Phone: +1 (410) 516 8546; Email: jimwest@jhu.edu

Authors

Valerie Rennoll − *Department of Electrical and Computer Engineering, Johns Hopkins University, Baltimore, Maryland 21218, United States;* orcid.org/0000-0003-2354-3377

Ian McLane − *Department of Electrical and Computer Engineering, Johns Hopkins University, Baltimore, Maryland 21218, United States*

Adebayo Eisape − *Department of Electrical and Computer Engineering, Johns Hopkins University, Baltimore, Maryland 21218, United States*

Drew Grant − *Department of Electrical and Computer Engineering, Johns Hopkins University, Baltimore, Maryland 21218, United States*

Helena Hahn − *Department of Electrical and Computer Engineering, Johns Hopkins University, Baltimore, Maryland 21218, United States*

Mounya Elhilali − *Department of Electrical and Computer Engineering, Johns Hopkins University, Baltimore, Maryland 21218, United States*

Complete contact information is available at:
https://pubs.acs.org/10.1021/acsabm.3c00359

Notes

The authors declare no competing financial interest.

REFERENCES

(1) Hiremath, N.; Kumar, V.; Motahari, N.; Shukla, D. An Overview of Acoustic Impedance Measurement Techniques and Future Prospects. *Metrology* **2021**, *1*, 17−38.

(2) Rossing, T. *Springer Handbook of Acoustics*; Springer, 2014.

(3) Zhu, K.; Ma, J.; Qi, X.; Shen, B.; Liu, Y.; Sun, E.; Zhang, R. Enhancement of Ultrasonic Transducer Bandwidth by Acoustic Impedance Gradient Matching Layer. *Sensors* **2022**, *22*, No. 8025.

(4) Vermarien, H.; van Vollenhoven, E. The recording of heart vibrations: a problem of vibration measurement on soft tissue. *Med. Biol. Eng. Comput.* **1984**, *22*, 168−178.

(5) Kuhn, C. Impact of extracorporeal shock waves on the human skin with cellulite: A case study of an unique instance. *Clin. Interventions Aging* **2008**, *3*, 201−210.

(6) Sabri, F.; Sebelik, M. E.; Meacham, R.; Boughter, J. D.; Challis, M. J.; Leventis, N. In Vivo Ultrasonic Detection of Polyurea Crosslinked Silica Aerogel Implants. *PLoS One* **2013**, *8*, No. e66348.

(7) Nowak, K. M.; Nowak, L. J. Experimental validation of the tuneable diaphragm effect in modern acoustic stethoscopes. *Postgrad. Med. J.* **2017**, *93*, 523−527.

(8) Mclane, I. M.; Emmanouilidou, D.; West, J.; Elhilali, M. Design and Comparative Performance of a Robust Lung Auscultation System for Noisy Clinical Settings. *IEEE J. Biomed. Health Inf.* **2021**, *25*, 2583−2594.

(9) Leng, S.; Tan, R. S.; Chai, K. T. C.; Wang, C.; Ghista, D.; Zhong, L. The electronic stethoscope. *BioMed. Eng. OnLine* **2015**, *14*, No. 66.

(10) Lee, S. H.; Kim, Y.-S.; Yeo, W.-H. Advances in Microsensors and Wearable Bioelectronics for Digital Stethoscopes in Health Monitoring and Disease Diagnosis. *Adv. Healthcare Mater.* **2021**, *10*, No. 2101400.

(11) Emmanouilidou, D.; McCollum, E. D.; Park, D. E.; Elhilali, M. Adaptive Noise Suppression of Pediatric Lung Auscultations With Real Applications to Noisy Clinical Settings in Developing Countries. *IEEE Trans. Biomed. Eng.* **2015**, *62*, 2279−2288.

(12) Yang, C.; Dai, N.; Wang, Z.; Cai, S.; Wang, J.; Hu, N. Cardiopulmonary auscultation enhancement with a two-stage noise cancellation approach. *Biomed. Signal Process. Control* **2023**, *79*, No. 104175.

(13) Liu, Y.; Norton, J. J. S.; Qazi, R.; Zou, Z.; Ammann, K. R.; Liu, H.; Yan, L.; Tran, P. L.; Jang, K.-I.; Lee, J. W.; Zhang, D.; Kilian, K. A.; Jung, S. H.; Bretl, T.; Xiao, J.; Slepian, M. J.; Huang, Y.; Jeong, J.-W.; Rogers, J. A. Epidermal mechano-acoustic sensing electronics for cardiovascular diagnostics and human-machine interfaces. *Sci. Adv.* **2016**, *2*, No. e1601185.

(14) Gupta, P.; Wen, H.; Di Francesco, L.; Ayazi, F. Detection of pathological mechano-acoustic signatures using precision accelerometer contact microphones in patients with pulmonary disorders. *Sci. Rep.* **2021**, *11*, No. 13427.

(15) Inan, O. T.; Baran Pouyan, M.; Javaid, A. Q.; Dowling, S.; Etemadi, M.; Dorier, A.; Heller, J. A.; Bicen, A. O.; Roy, S.; De Marco,

T.; Klein, L. Novel Wearable Seismocardiography and Machine Learning Algorithms Can Assess Clinical Status of Heart Failure Patients. *Circ.: Heart Failure* **2018**, *11*, No. e004313.

(16) Lapi, S.; Lavorini, F.; Borgioli, G.; Calzolai, M.; Masotti, L.; Pistolesi, M.; Fontana, G. A. Respiratory rate assessments using a dual-accelerometer device. *Respir. Physiol. Neurobiol.* **2014**, *191*, 60−66.

(17) Hu, Y.; Kim, E. G.; Cao, G.; Liu, S.; Xu, Y. Physiological Acoustic Sensing Based on Accelerometers: A Survey for Mobile Healthcare. *Ann. Biomed. Eng.* **2014**, *42*, 2264−2277.

(18) Mohd-Yasin, F.; Nagel, D. J.; Korman, C. E. Noise in MEMS. *Meas. Sci. Technol.* **2009**, *21*, No. 012001.

(19) Sujatha, P. C. *Vibration and Acoustics: Measurement and Signal Analysis*; McGraw-Hill Education, 2010.

(20) Mallegni, N.; Molinari, G.; Ricci, C.; Lazzeri, A.; La Rosa, D.; Crivello, A.; Milazzo, M. Sensing Devices for Detecting and Processing Acoustic Signals in Healthcare. *Biosensors* **2022**, *12*, No. 835.

(21) Joyashiki, T.; Wada, C. Validation of a Body-Conducted Sound Sensor for Respiratory Sound Monitoring and a Comparison with Several Sensors. *Sensors* **2020**, *20*, No. 942.

(22) Lee, S. H.; Kim, Y.-S.; Yeo, M.-K.; Mahmood, M.; Zavanelli, N.; Chung, C.; Heo, J. Y.; Kim, Y.; Jung, S.-S.; Yeo, W.-H. Fully portable continuous real-time auscultation with a soft wearable stethoscope designed for automated disease diagnosis. *Sci. Adv.* **2022**, *8*, No. eabo5867.

(23) Cotur, Y.; Kasimatis, M.; Kaisti, M.; Olenik, S.; Georgiou, C.; Güder, F. Stretchable Composite Acoustic Transducer for Wearable Monitoring of Vital Signs. *Adv. Funct. Mater.* **2020**, *30*, No. 1910288.

(24) Lee, K.; Ni, X.; Lee, J. Y.; Arafa, H.; Pe, D. J.; Xu, S.; Avila, R.; Irie, M.; Lee, J. H.; Easterlin, R. L.; Kim, D. H.; Chung, H. U.; Olabisi, O. O.; Getaneh, S.; Chung, E.; Hill, M.; Bell, J.; Jang, H.; Liu, C.; Park, J. B.; Kim, J.; Kim, S. B.; Mehta, S.; Pharr, M.; Tzavelis, A.; Reeder, J. T.; Huang, I.; Deng, Y.; Xie, Z.; Davies, C. R.; Huang, Y.; Rogers, J. A. Mechano-acoustic sensing of physiological processes and body motions via a soft wireless device placed at the suprasternal notch. *Nat. Biomed. Eng.* **2020**, *4*, 148−158.

(25) Gupta, P.; Moghimi, M. J.; Jeong, Y.; Gupta, D.; Inan, O. T.; Ayazi, F. Precision wearable accelerometer contact microphones for longitudinal monitoring of mechano-acoustic cardiopulmonary signals. *npj Digital Med.* **2020**, *3*, No. 19.

(26) Ji, Z.; Zhang, M. Highly sensitive and stretchable piezoelectric strain sensor enabled wearable devices for real-time monitoring of respiratory and heartbeat simultaneously. *Nanotechnol. Precis. Eng.* **2022**, *5*, No. 013002.

(27) Yilmaz, G.; Rapin, M.; Pessoa, D.; Rocha, B. M.; de Sousa, A. M.; Rusconi, R.; Carvalho, P.; Wacker, J.; Paiva, R. P.; Chételat, O. A Wearable Stethoscope for Long-Term Ambulatory Respiratory Health Monitoring. *Sensors* **2020**, *20*, No. 5124.

(28) Qu, M.; Chen, X.; Yang, D.; Li, D.; Zhu, K.; Guo, X.; Xie, J. Monitoring of physiological sounds with wearable device based on piezoelectric MEMS acoustic sensor. *J. Micromech. Microeng.* **2022**, *32*, No. 014001.

(29) Chen, H.; Yu, S.; Liu, H.; Liu, J.; Xiao, Y.; Wu, D.; Pan, X.; Zhou, C.; Lei, Y.; Liu, S. A two-stage amplified PZT sensor for monitoring lung and heart sounds in discharged pneumonia patients. *Microsyst. Nanoeng.* **2021**, *7*, No. 55.

(30) Liu, Z.; Li, H.; Shi, B.; Fan, Y.; Wang, Z. L.; Li, Z. Wearable and Implantable Triboelectric Nanogenerators. *Adv. Funct. Mater.* **2019**, *29*, No. 1808820.

(31) Liu, Z.; Zhao, Z.; Zeng, X.; Fu, X.; Hu, Y. Expandable microsphere-based triboelectric nanogenerators as ultrasensitive pressure sensors for respiratory and pulse monitoring. *Nano Energy* **2019**, *59*, 295−301.

(32) Ma, Y.; Zheng, Q.; Liu, Y.; Shi, B.; Xue, X.; Ji, W.; Liu, Z.; Jin, Y.; Zou, Y.; An, Z.; Zhang, W.; Wang, X.; Jiang, W.; Xu, Z.; Wang, Z. L.; Li, Z.; Zhang, H. Self-Powered, One-Stop, and Multifunctional Implantable Triboelectric Active Sensor for Real-Time Biomedical Monitoring. *Nano Lett.* **2016**, *16*, 6042−6051.

(33) Cui, J.; Li, Y.; Yang, Y.; Shi, P.; Wang, B.; Wang, S.; Zhang, G.; Zhang, W. Design and optimization of MEMS heart sound sensor based on bionic structure. *Sens. Actuators, A* **2022**, *333*, No. 113188.

(34) Zhao, Z.; Feng, X.; Chen, X.; Dai, L. L.; Xu, Y. A wearable mechano-acoustic sensor based on electrochemical redox reaction for continuous cardiorespiratory monitoring. *Appl. Phys. Lett.* **2021**, *118*, No. 023703.

(35) Hosono, Y.; Itsumi, K. Effects of Ceramic Nanopowder Dopants on Acoustic Attenuation Properties of Silicone Rubber Lens for Medical Echo Probe. *Jpn. J. Appl. Phys.* **2007**, *46*, 4784.

(36) Zell, K.; Sperl, J. I.; Vogel, M. W.; Niessner, R.; Haisch, C. Acoustical properties of selected tissue phantom materials for ultrasound imaging. *Phys. Med. Biol.* **2007**, *52*, N475−N484.

(37) Guillermic, R.-M.; Lanoy, M.; Strybulevych, A.; Page, J. A PDMS-based broadband acoustic impedance matched material for underwater applications. *Ultrasonics* **2019**, *94*, 152−157.

(38) Cafarelli, A.; Verbeni, A.; Poliziani, A.; Dario, P.; Menciassi, A.; Ricotti, L. Tuning acoustic and mechanical properties of materials for ultrasound phantoms and smart substrates for cell cultures. *Acta Biomater.* **2017**, *49*, 368−378.

(39) Kressmann, R.; Sessler, G.; Gunther, P. Space-charge electrets. *IEEE Trans. Dielectr. Electr. Insul.* **1996**, *3*, 607−623.

(40) *JMP*, version 15.2; Pro. SAS Institute Inc.: Cary, NC, 1989.

(41) Hughes, S. W. Archimedes revisited: a faster, better, cheaper method of accurately measuring the volume of small objects. *Phys. Educ.* **2005**, *40*, 468−474.

(42) Jones, F.; Harris, G. ITS-90 density of water formulation for volumetric standards calibration. *J. Res. Natl. Inst. Stand. Technol.* **1992**, *97*, 335.

(43) Bamber, J. C. *Physical Principles of Medical Ultrasonics*; John Wiley & Sons, Ltd., 2004; pp 167−190.

(44) Cuccaro, R.; Musacchio, C.; Giuliano Albo, P. A.; Troia, A.; Lago, S. Acoustical characterization of polysaccharide polymers tissue-mimicking materials. *Ultrasonics* **2015**, *56*, 210−219.

(45) Ginzel, E.; Turnbull, B. Determining Approximate Acoustic Properties of Materials. *e-J. Nondestr. Test.* **2016**, *21*, 1−10.

(46) He, P.; Zheng, J. Acoustic dispersion and attenuation measurement using both transmitted and reflected pulses. *Ultrasonics* **2001**, *39*, 27−32.

(47) McClements, D. J.; Fairley, P. Ultrasonic pulse echo reflectometer. *Ultrasonics* **1991**, *29*, 58−62.

(48) Menikou, G.; Damianou, C. Acoustic and thermal characterization of agar based phantoms used for evaluating focused ultrasound exposures. *J. Ther. Ultrasound* **2017**, *5*, No. 14.

(49) Ceh, D.; Peters, T. M.; Chen, E. C. S. In *Acoustic Characterization of Polyvinyl Chloride and Self-Healing Silicone as Phantom Materials*, Proceedings Volume 9412, Medical Imaging 2015: Physics of Medical Imaging, Orlando, Florida, 2015; 94123G.

(50) Madsen, E. L.; Frank, G. R.; Carson, P. L.; Edmonds, P. D.; Frizzell, L. A.; Herman, B. A.; Kremkau, F. W.; O'Brien, W. D.; Parker, K. J.; Robinson, R. A. Interlaboratory comparison of ultrasonic attenuation and speed measurements. *J. Ultrasound Med.* **1986**, *5*, 569−576.

(51) Marczak, W. Water as a standard in the measurements of speed of sound in liquids. *J. Acoust. Soc. Am.* **1997**, *102*, 2776−2779.

(52) Bian, J.; Wang, Y.; Liu, Z.; Shen, M.; Zhao, H.; Sun, Y.; Zhu, J. Ultra-wideband underwater acoustic transducer with a gradient impedance matching layer. *Appl. Acoust.* **2021**, *175*, No. 107789.

(53) Bakhtiari-Nejad, M.; Hajj, M. R.; Shahab, S. Dynamics of acoustic impedance matching layers in contactless ultrasonic power transfer systems. *Smart Mater. Struct.* **2020**, *29*, No. 035037.

(54) Rennoll, V.; McLane, I.; Elhilali, M.; West, J. E. Optimized Acoustic Phantom Design for Characterizing Body Sound Sensors. *Sensors* **2022**, *22*, No. 9086.

(55) Le Duff, A.; Plantier, G.; Valière, J. C.; Gazengel, B. Acoustic velocity measurement by means of Laser Doppler Velocimetry: Development of an Extended Kalman Filter and validation in free-field measurement. *Mech. Syst. Signal Process.* **2016**, *70−71*, 832−852.

(56) Sovijärvi, A. R. A.; Vanderschoot, J.; Earis, J. E. *Computerized Respiratory Sound Analysis (CORSA): Recommended Standards for Terms and Techniques: ERS Task Force Report*; Munksgaard, 2000.

(57) REW, version 5.20.4, John Mulcahy.

(58) Müller, S. In *Handbook of Signal Processing in Acoustics*; Havelock, D.; Kuwano, S.; Vorländer, M., Eds.; Springer: New York, NY, 2008; pp 65−85.

(59) *The BBC Sound Effects Library Original Series*, 2006.

(60) Varga, A. P.; Steeneken, H. J. M.; Tomlinson, M.; Jones, D. *The NOISEX-92 Study on the Effect of Additive Noise on Automatic Speech Recognition*, Technical Report; Speech Research Unit, Defense Research Agency: Malvern, U.K., 1992.

(61) *Nursing Know-How. Evaluating Heart & Breath Sounds*; Wolters Kluwer Health/Lippincott Williams & Wilkins: Philadelphia, 2022.

(62) Lauwers, E. Novel Outcome Measures for Cystic Fibrosis in a Changing World: Functional Respiratory Imaging and Computer Aided Lung Sound Analysis; University of Antwerp, 2022.

(63) Ma, J.; Hu, Y.; Loizou, P. C. Objective measures for predicting speech intelligibility in noisy conditions based on new band-importance functions. *J. Acoust. Soc. Am.* **2009**, *125*, 3387.

(64) Nowak, L. J.; Nowak, K. M. Sound differences between electronic and acoustic stethoscopes. *BioMed. Eng. OnLine* **2018**, *17*, No. 104.

(65) Marques, A.; Oliveira, A. In *Breath Sounds: From Basic Science to Clinical Practice*; Priftis, K. N.; Hadjileontiadis, L. J.; Everard, M. L., Eds.; Springer International Publishing: Cham, 2018; pp 181−206.

(66) Ahmed, S. A.; Adamopoulos, S. Acoustic properties of modified wood under different humid conditions and their relevance for musical instruments. *Appl. Acoust.* **2018**, *140*, 92−99.

(67) Sessler, G. M. In *Electrets*; Sessler, G. M., Ed.; Topics in Applied Physics; Springer: Berlin, Heidelberg, 1987; pp 13−80.

(68) Malmberg, L. P.; Pesu, L.; Sovijärvi, A. R. Significant differences in flow standardised breath sound spectra in patients with chronic obstructive pulmonary disease, stable asthma, and healthy lungs. *Thorax* **1995**, *50*, 1285−1291.

(69) Klum, M.; Stehling, J.; Pielmus, A.; Tigges, T.; Orglmeister, R. Validation System for Digital Stethoscopes. *Curr. Dir. Biomed. Eng.* **2019**, *5*, 261−264.

(70) Lawson, N.; Thompson, K.; Saunders, G.; Saiz, J.; Richardson, J.; Brown, D.; Ince, N.; Caldwell, M.; Pope, D. Sound Intensity and Noise Evaluation in a Critical Care Unit. *Am. J. Crit. Care* **2010**, *19*, e88−e98.